Design and Development of Strategies and Structures for Wing Morphing

J. Vale, A. Leite, F. Lau and A. Suleman[1]
Instituto Superior Técnico, Lisbon, Portugal

ABSTRACT

A morphing concept of a telescopic wing with airfoil shape change capability was designed and analyzed using coupled fluid-structure interaction. Morphing strategies for drag reduction were obtained. Morphing benefits were estimated in terms of extra loading at take-off speed and drag reduction with speed. Additional loading upto 15 N was attained and drag reduction varied from 1.7 to 12 N for a 100 N aircraft. A preliminary experimental telescopic wing based on this concept and geometry without airfoil shape change capability was built and ground--tested in terms of actuation energy and structural loads. Actuation energy and actuation time results are promising for morphing in level flight. Functional problems such as closing a structural gap in the wing's leading edge are still to be solved before flight testing. Future work will include design of airfoil morphing mechanisms to assemble in next versions of the experimental morphing wing.

INTRODUCTION

Birds always inspired man to fly. They are the outcome of millions of years of nature's evolution. The resemblance between an airplane and a bird at first glance is very high but bird's morphology is not as rigid as airplane morphology. They can smoothly change the shape of all their body parts to achieve optimum performance in various flight conditions such as high speed dash and low speed loiter and increased manoeuvrability.

Morphing technology is intended to approximate aircraft adaptability to different flight conditions, by changing aircraft shape in different stages of flight, as birds do, to allow an expansion of the flight envelope, an increase in efficiency of flight and multiple mission profiles to be performed by the same aircraft.

Morphing technologies are a topic of recent research interest in aerospace engineering, although most of the concepts used are not new. Wilbur Wright was looking in 1899 for a way to control the roll of the Wright B flyer by twisting the aircraft wing to produce lateral control. This is now called wing warping.

Concepts like span camber variation[1], lateral control via variable cant angle winglets[2], variable span wings[3], morphing airfoils [4,10], variable wing sweep[5], simultaneous variable span and chord[6,7,8], pneumatic telescopic wings[9], rubber skin wings[13] have been studied for some years.

Recent developments have led to wind tunnel testing and validation of two different concepts: a folding wing from Lockeed Martin morphing concept[16] and the NextGen batwing morphing concept[11,12,15]. The NextGen prototype has flown successfully and allowed variable sweep and span, while also increasing the wing area in some configurations. It had a silicon skin which could stretch and increase wing area but it couldn't maintain an efficient airfoil shape. It was also impossible to quantify the benefits of the morphing strategies due to the impossibility to obtain drag data from the wind tunnel scale because

[1] Corresponding author: suleman@uvic.ca; Professor, University of Victoria, BC, Canada; AVT Panel Member.

of the heavy weight of the prototype.

In this paper we present the computational design and analysis of a telescopic wing, as well as some experimental structural results. First the morphing concept is explained and both computational and experimental models are described, then computational and experimental results are presented and discussed in terms of morphing strategies and benefits, and in terms of actuation energy and constructive solutions, and finally the main conclusions are highlighted.

MORPHING WING CONCEPT

The morphing wing concept presented in this paper consists of a variable span wing which allows airfoil shape change of all wing sections simultaneously between two different airfoils, as shown in figure 1. The wing's performance is to be compared to the original fixed wing installed on an RPV demonstrator (Antex-X2) performance.

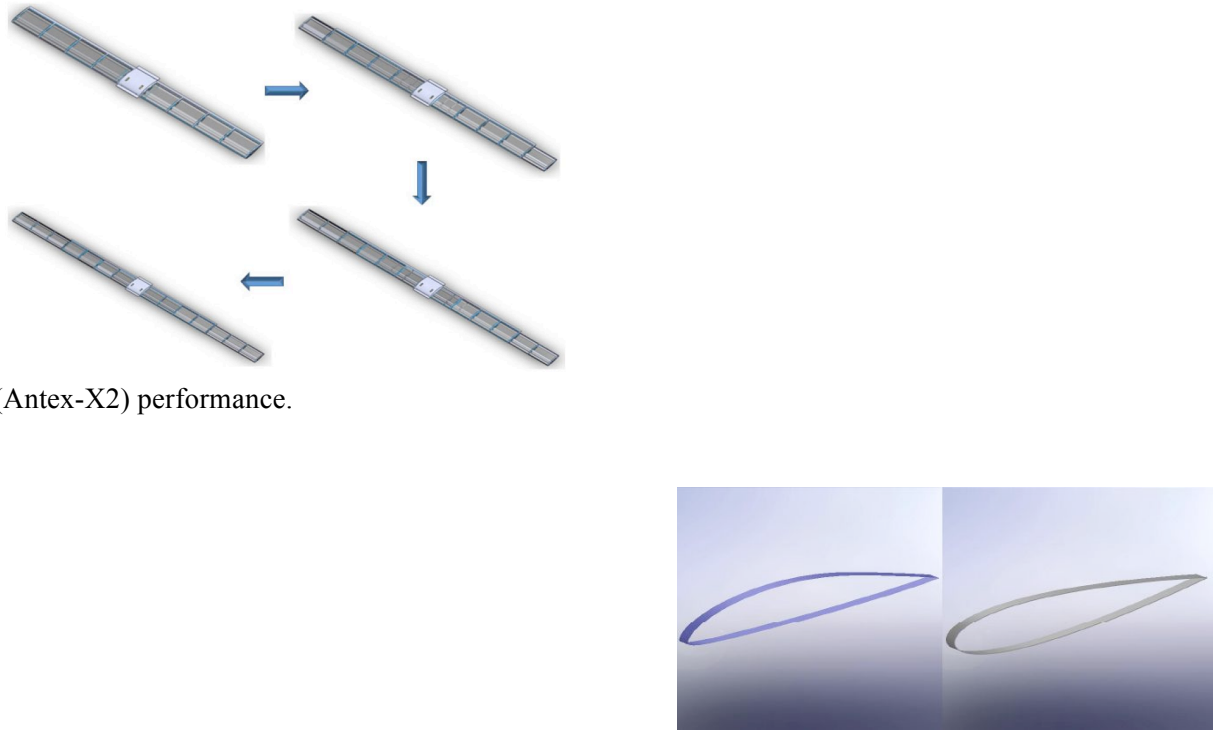

Figure 1. Different span configurations (left) and Eppler 434 and NACA 0012 airfoil shapes (right) of the morphing wing.

The telescopic wing can continuously change the wing span as it has an inner wing that slides in and out of the outer wing. The inner wing and the outer wing are defined as having 1m span (half wing span) each and the inner wing can be deployed up to a maximum of 0.75 m.

The wing can also change the airfoil shape independently of the span variation. In the study of airfoil shape change, it is assumed that it can only change between two different and specific airfoils; a high speed airfoil and a low speed airfoil and that all sections of the wing change to the same airfoil shape simultaneously. The airfoil chosen for low speed flight was the Eppler-434 and for high speed flight was the Naca-0012 as presented in figure 1. These airfoils were chosen based on construction restrictions and good sense: the inner wing has to fit inside the outer wing and so airfoils with chord line crossing the contour of the airfoil should be discarded if the inner wing chord length is to be as close to the outer wing

chord length as possible; also for low speed flight an airfoil with high maximum lift coefficient should be chosen, as is the Eppler-434, and for high speed flight a thin and symmetric airfoil is usually a good choice.

Table 1 summarizes the different configurations of the morphing wing analysed in the computational study as well as the original RPV wing geometry.

Table 1. Summary of RPV morphing and original wing configurations.

Airfoil	Outer wing chord (m)	Inner wing chord (m)	Half wing span (m)
NACA 0012	0.22	0.20	1.00, 1.25, 1.50, 1.75
Eppler 434	0.22	0.20	1.00, 1.25, 1.50, 1.75
Wortman FX-63	0.33	Not applicable	1.00

MORPHING STRUCTURE DESCRIPTION

The structural solution adopted to achieve the morphing capability described in the previous section consists of a hollow outer wing which supports loadings having leading and trailing edge composite carbon fibre reinforcement as well as composite carbon fibre reinforcements evenly spaced along the span to substitute conventional ribs (figure 2).

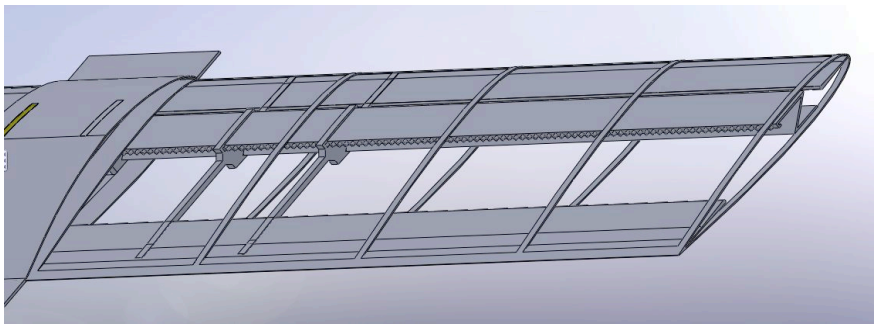

Figure 2: Outer wing

From the leading and trailing edge to the interior of the outer wing there are carbon fibre composite plates for support and sliding guidance to the inner wing. Also inside the outer wing there are sliding ribs and a spar. The sliding ribs slide along the spar as the inner wing is extended to increase the span, in order to transmit some of the loading to the spar.

The inner wing is a normal wing with fixed ribs and a fixed spar with the exception that it is open on the leading and trailing edge to fit the leading and trailing edge plates of the outer wing and that the inner wing spar fits and slides along the outer wing spar (figure 3, the leading and trailing edge openings are not shown).

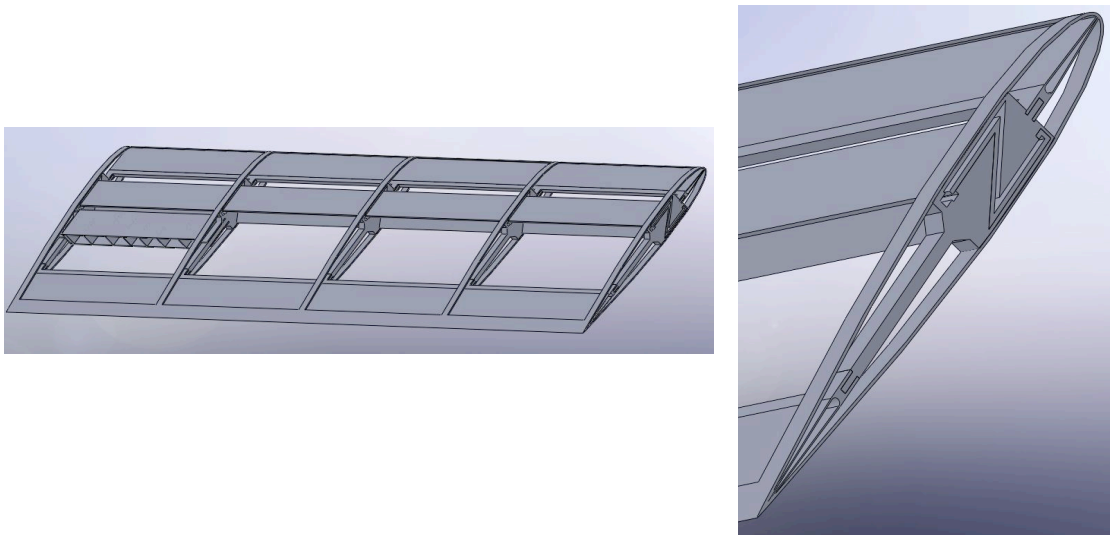

Figure 3: Inner wing (left) and inner wing detail (right)

Both wings are covered with carbon fibre composite shells and actuation is done by attaching the actuation mechanism to the inner wing and forcing the relative movement between inner wing and outer wing spars.

Figure 4 illustrates the morphing wing span increase sequence.

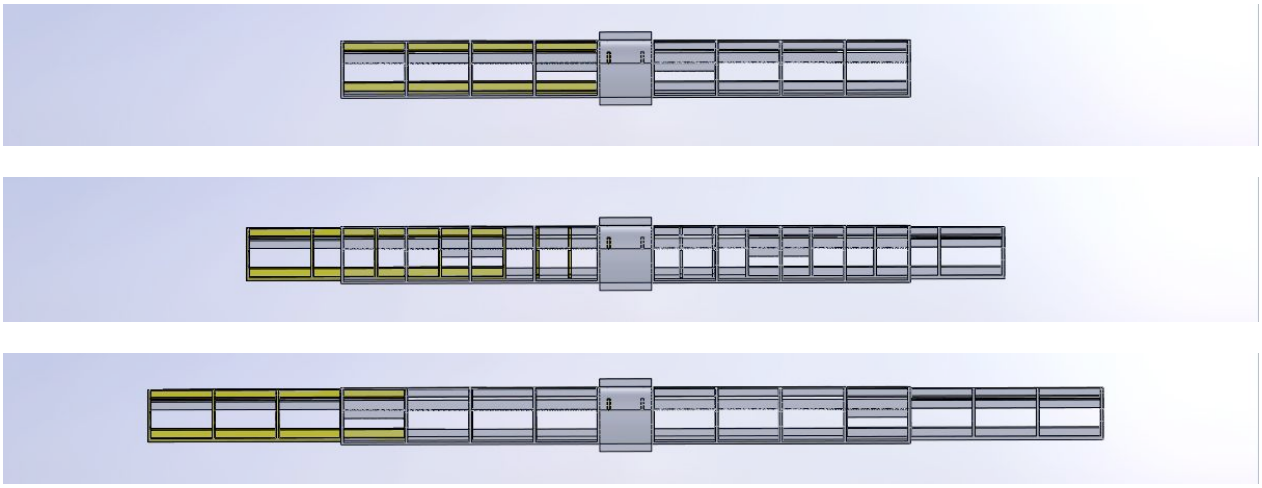

Figure 4: Span increase sequence

To compare this wing to the original RPV wing, designed for 98N of maximum take of weight, the structure is to withstand approximately 290N (145 N for half wing) of lift and the respective drag, corresponding to approximately 3g loading when fully extended.

COMPUTATIONAL MODELLING

Coupled field analysis

Coupled field analysis or multifield analysis is a combination of analysis from different engineering

disciplines that interact with each other to solve a global engineering problem, where the input of one field depends on the results from another. There are engineering problems where there is no need to interact between the two fields solutions. For example, this usually occurs in thermal stress analysis, where the temperature field introduces thermal strains in the structural field, but generally the structural strains do not affect the temperature distribution. However, in a fluid-structure analysis, the fluid pressure causes the structure to deform, which in turn causes the fluid solution to change and therefore interaction between the two physic fields is required to achieve a converged solution.

Ansys® multifield analysis using code coupling

In a coupled field analysis using multiple codes (Ansys® and Ansys-CFX®) there are two codes distributed by two programs. In the case presented here, the Ansys® code always functions as the master and the Ansys-CFX® as the slave. Since the solid models and respective mesh in the Ansys® and Ansys-CFX® models are independent, the master, Ansys®, reads all commands, collects the interface meshes from the Ansys-CFX® code and proceeds to the mapping process.

The mapping consists of an interpolation of the two distinct meshes to transfer loads between the interface surfaces. The Ansys® code is also responsible for communicating time and stagger loop controls to Ansys-CFX®. Time controls are used if a transient analysis is being executed and provides a way for Ansys® and Ansys-CFX® to track the progress of real time during simulation.

Stagger loops consist of coupling iterations between the two fields until reaching some convergence criteria. For example, a transient analysis usually needs a series of coefficient loops in each time step; in other words, for a specific time, there is the need of a series of interactions between the two fields, in order to achieve the converged solution. During every stagger loop, each field solver collects the required loads from the other field solver and then solves its physics field. If global convergence of the load transfer is not achieved another stagger loop is performed.

It is important to refer that Ansys® and the Ansys-CFX® fields can be solved simultaneously or sequentially, as presented in figure 5. Weakly coupled fields can be solved simultaneously, and the overall simulation time may decrease because no field solver must wait for the results from the other field solver. However, if the fields are strongly coupled, the simultaneous solution procedure may destabilize the solution process because less recent results are applied in each field solver and therefore the sequential solution was chosen for this analysis.

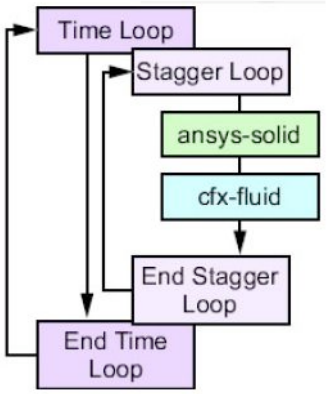

Figure 5: Ansys® and Ansys-CFX® fields solved sequentially procedure must be applied.

To accomplish this analysis one model for each field had to be created. Thus one model was created in Ansys® for the structural field and one was created on Ansys® ICEM-CFD for the fluid field.

To model a wing morphing with airfoil shape variation and span variation a model with continuous and independent airfoil variation and span variation should be created. This would be extremely complex, even more with the inclusion of the fluid/structure interaction which is the base of this analysis. The fluid field mesh elements had to be able to adapt to a continuous change in the span of the wing in the order of 75%. This would cause the elements to deform unacceptably and compromise the analysis. One solution would be to automatically generate a new fluid field mesh every time the previous mesh was not able to comply with element quality demands. Since there is no such algorithm in the commercial codes and there is no known solution for this problem, a simpler approach was used. We have replaced the continuous span variation model with continuous airfoil shape changing with several discrete models that simulate in a specified configuration the wing in study. These configurations are representative of the wing behaviour in static conditions and are shown in table 1 above.

The models were used first for the dimensioning of the morphing wing structure and then for the aerodynamic performance quantification. Relevant properties of the materials used are shown in table 2.

Table 2: Properties of structural model materials

Material	Fibre volume fraction (%)	Young's Modulus (longitudinal) (GPa)	Young's Modulus (transverse) (GPa)
Carbon Composite Shell	55-60	120-140	10
Carbon Composite Reinforcements	50	70	70

Detailed descriptions of the model characteristics and analysis procedures can be found in [14].

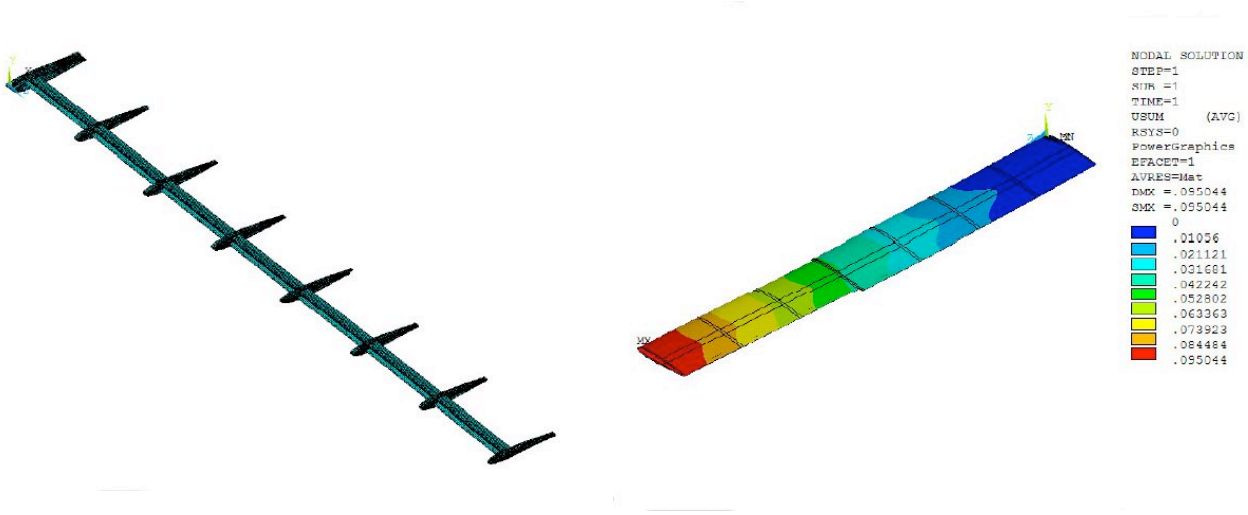

Figure 6: Internal structure mesh (left) and wing deformation at approx. 3g loading (145.3N, 8º AOA fully extended)

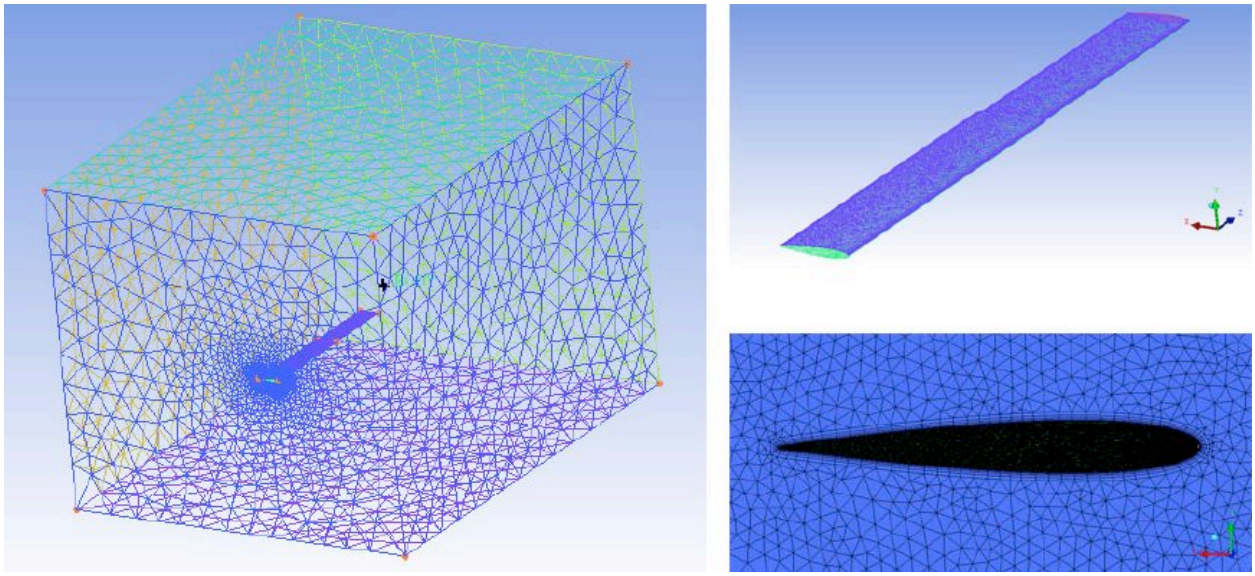

Figure 7: Fluid field model mesh

EXPERIMENTAL MODEL

An experimental morphing wing is near to completion at the Portuguese Air Force Academy in cooperation with IST for flight tests. This model is based on the morphing concept described above but it differs from the computational model in some aspects, mainly because of construction simplifications. It doesn't include airfoil shape change capability.

The span increase capability of the experimental wing is the same as the model. The chosen airfoil for this morphing wing was the NACA 0012 and the inner and outer wing chords are 0.21 m and 0.28 m respectively.

The wing shells are made of two layers of 220 g/m^2 unidirectional carbon fibre composite and 1mm thick balsa wood. The plates that support the inner wing are made of aluminium and the spars are made of bidirectional carbon fibre composite. There are no sliding ribs or shell reinforcements.

Actuation is based on electric motors attached to the inner wing that force it to slide along the spars in a rack and pinion mode, the outer wing spar being the rack.

The inner wing is open at the leading and trailing edge, as referred before. A feasible solution to cover the inner wing's leading edge as it deploys and uncover the leading edge as it retracts is still to be found.

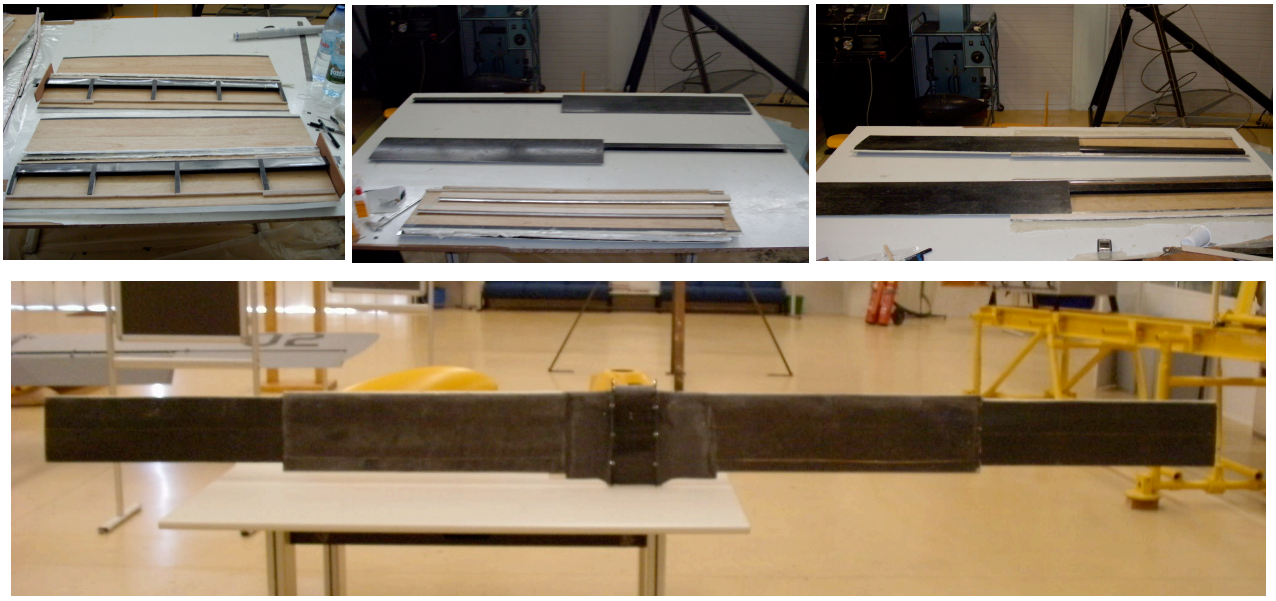

Figure 8: Experimental morphing wing construction (up) and final assembly fully extended (down)

Table 3 shows the geometry of the experimental wing and its possible variations.

Table 3. Experimental wing geometry.

Dimension (half wing)	Quantity
Inner wing chord	0.210 m
Inner wing span	0.950 m
Outer wing chord	0.280 m
Outer wing span	1.000 m
Central section span	0.144
Span variation	2.144 - 3.644 m
Span increase	Up to 70.0%
Area Variation	0.600 – 0.915 m^2
Area increase	Up to 52.5%
Aspect ratio variation	7.66 – 14.51
Aspect ratio increase	Up to 89.4%

RESULTS

Computational results

The final model dimensions which comply with the loading requirements without risk of failure are summarized in table 4:

Table 4. Summary of final morphing wing dimensions.

Dimension (half wing)	Quantity
Wing shell sections thickness	0.0002 m
Wing composite reinforcements thickness	0.0010 m
Wing composite reinforcements width	0.0050 m
Nº of shell reinforcements outer wing	5
Nº of shell reinforcements inner wing	5
Nº of sliding ribs outer wing	2
Nº of fixed ribs outer wing	1
Nº of fixed ribs inner wing	5
Ribs material	Carbon fiber composite reinforcement
Wing weight	0.867 Kg

Figure 9 shows the polar CD(CL) curves for the eight different morphing wing configurations at level flight at sea level. Each curve represents a different combination of span and airfoil shape. The lift and drag coefficients are calculated using the maximum wing area configuration of the morphing wing.

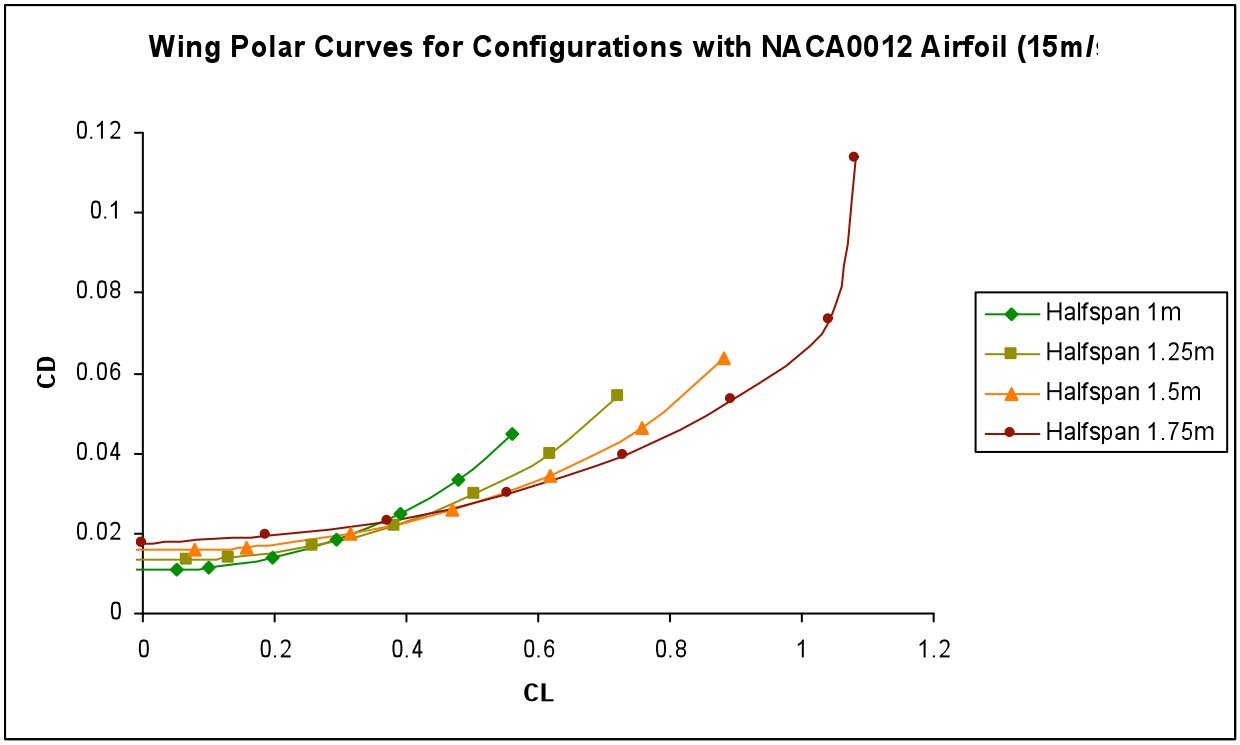

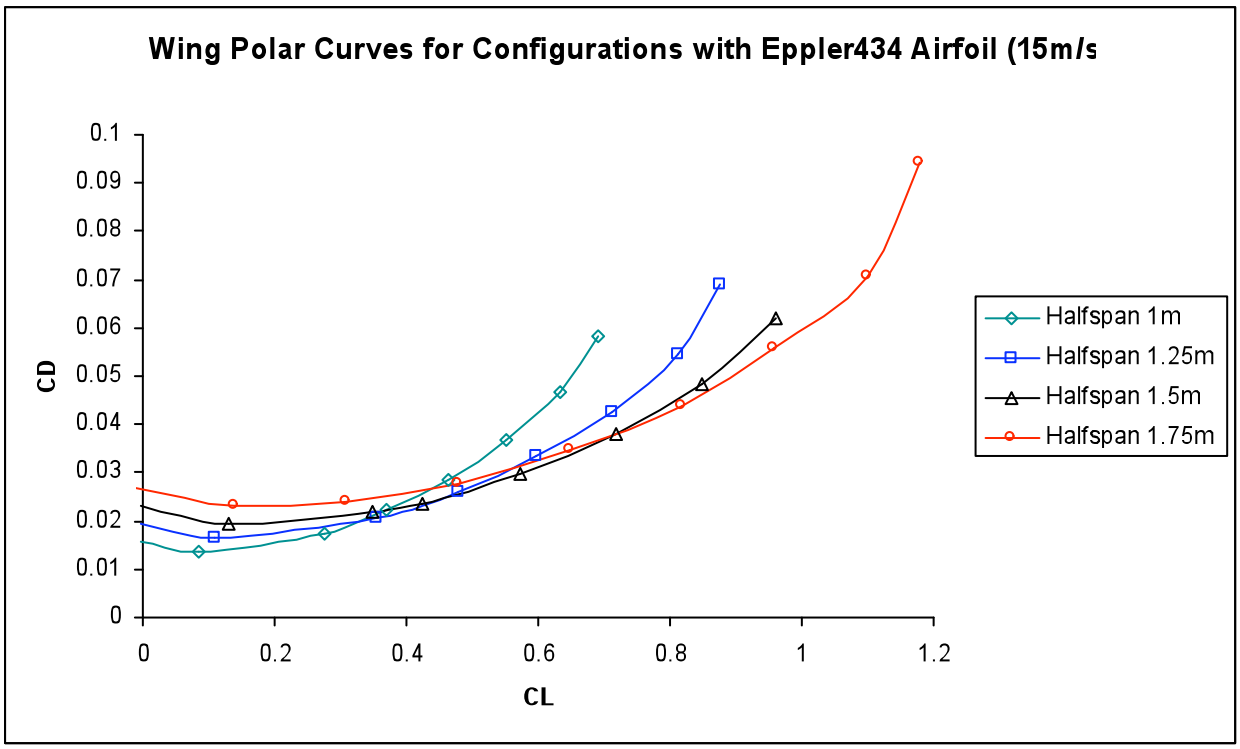

Figure 9: CD(CL) curves for different span configurations for the NACA0012 airfoil (up) and the Epller 434 airfoil (down) at 15 m/s

As expected, different configurations are more efficient than others, depending on the CL required for

flight. Because the CL and CD coefficients are calculated using always the same wing area, the required CL for level flight depends directly on the airspeed. As airspeed increases, the required CL decreases, and we start finding points were the curves cross, which means that a new configuration will reduce drag for that airspeed and higher airspeeds.

Therefore we can create an approximation to the optimum polar curve for the morphing wing with span variation capability for a fixed airfoil, by selecting the sections of the polar curves between the crossing points with the adjacent configurations polar curves, as shown in figure 10.

Using the same reasoning and assuming that airfoil shape change is possible, we can create a new approximation to the optimum polar curve for the morphing wing with span and airfoil variation capability, as shown in figure 11

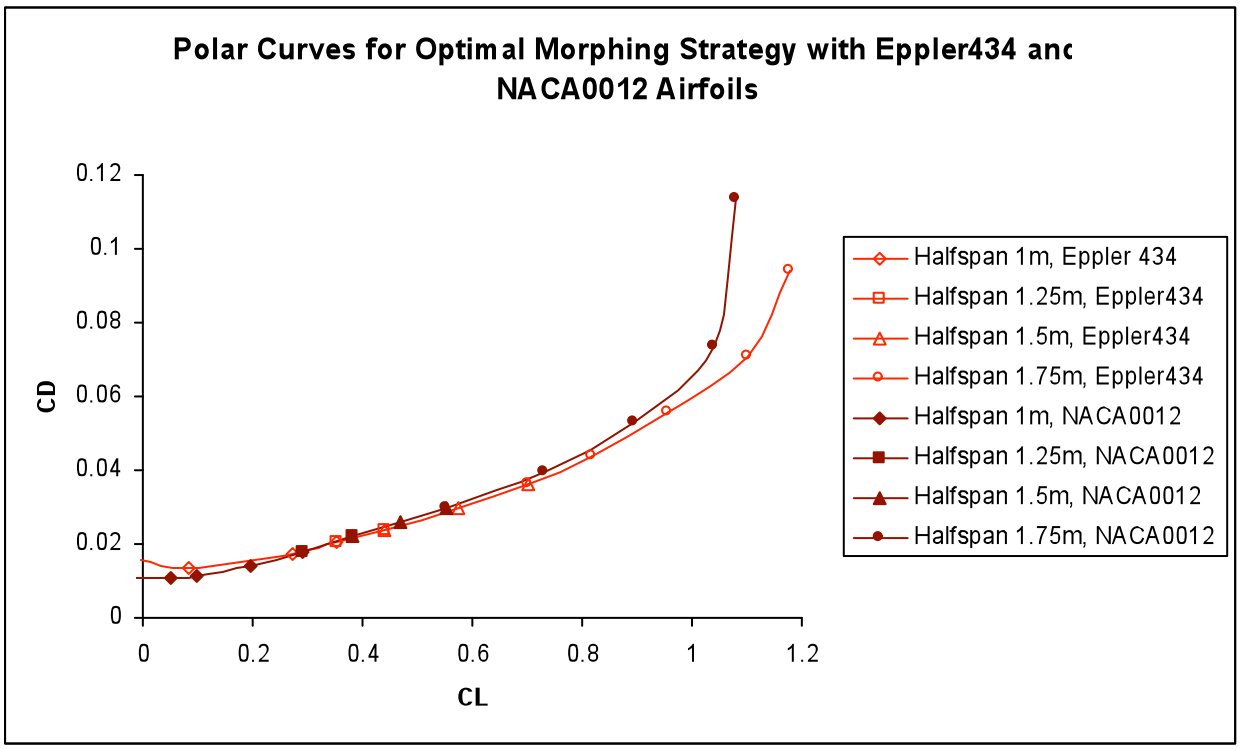

Figure 10: Optimum polar curves for fixed airfoil and variable span morphing wing configurations.

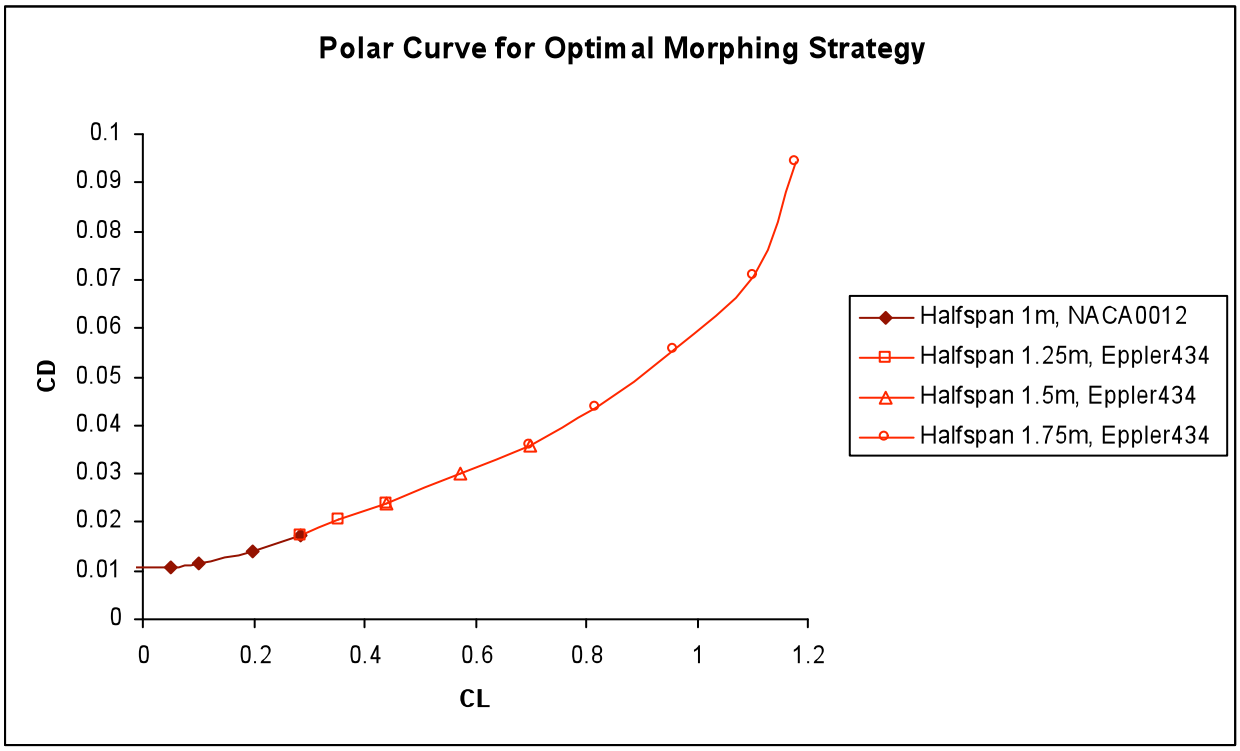

Figure 11: Optimum polar curve for variable airfoil and span morphing wing configurations.

Figure 11 clearly shows the morphing strategy for level flight of an aircraft with this morphing wing. The aircraft should take off with maximum span and with the Eppler-434 airfoil configuration, increase speed maintaining the airfoil and reducing the span and change the airfoil to NACA0012 when the inner wing is fully retracted at high speed. The inverse strategy should be used as speed decreases. Table 5 summarizes the morphing strategy.

Table 5. Summary of morphing strategy for level flight.

CL	Airfoil	Half span (m)	AOA (º)	CD
≤0.284	NACA 0012	1.00	0-5.92	0.011-0.017
0.284-0.441	Eppler 434	1.25	0.85-3.62	0.017-0.024
0.441-0.702	Eppler 434	1.5	2.28-6.00	0.024-0.036
0.702-1.230	Eppler 434	1.75	5.01-12	0.036-0.086

Comparing the optimum morphing wing polar curve to the original RPV wing one, we can expect the morphing wing to outperform the original wing in all performance parameters that depend on drag reduction (figure 12).

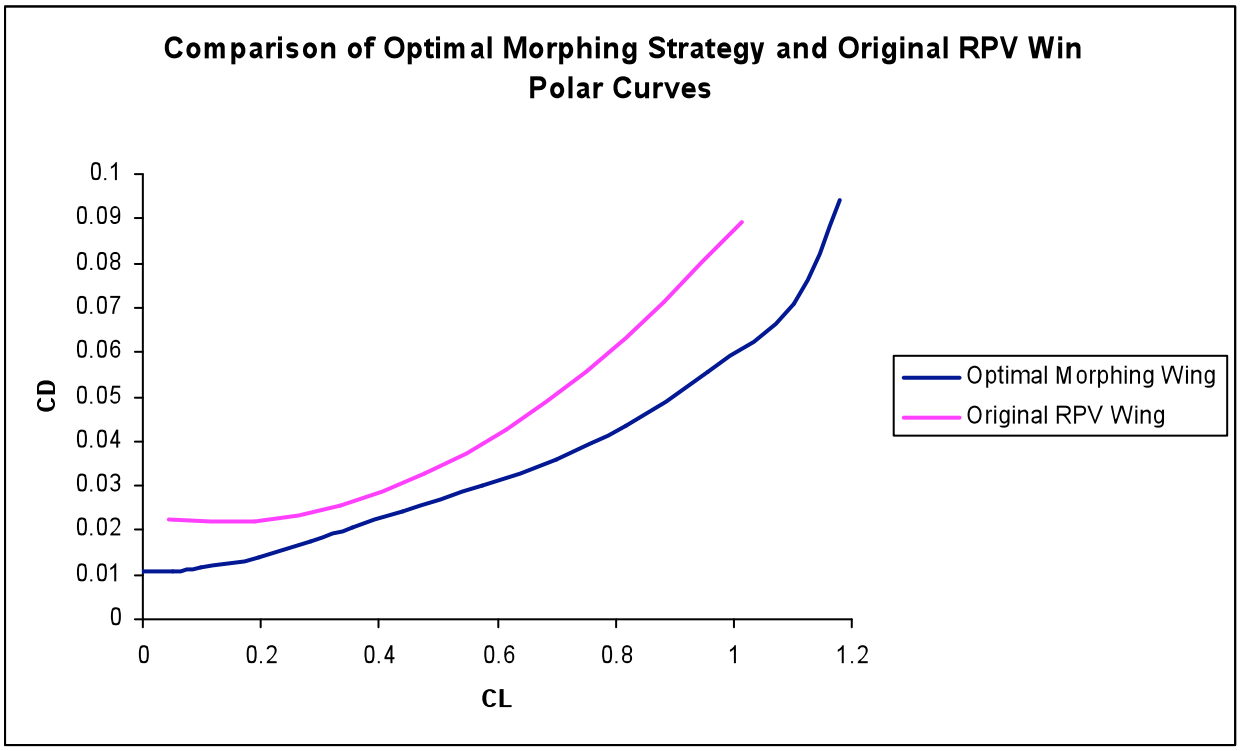

Figure 12: Polar curves comparison between optimum morphing wing and original RPV wing

From this comparison we can estimate the possible increase in payload by calculating the difference between CL values from the original and morphing wing curves for a fixed CD value, or a decrease in wing drag by calculating the difference in CD values from the original and morphing wing curves for a fixed CL value, which translates into reduced fuel consumption. Figure 13 shows these estimates.

The graphics in figure 13 show the two possible benefits from the morphing wing. The first shows how much extra weight the aircraft can carry at a specific take off speed. This extra weight can be either extra structural weight from the morphing mechanism and/or extra payload. When the difference between morphing and original wing weights exceeds this amount the payload must be reduced, and the morphing benefits or penalties become a compromise between the payload reduction and the drag reduction at higher speeds, which is the second possible benefit from this morphing concept.

In fact, the possible weight increase at take off is only a comparison between different fixed wing configurations. For a fixed wing optimized for lift at low speeds the morphing wing would be outperformed and it would have to be lighter than the optimized fixed wing. Nevertheless the morphing wing would outperform the optimized wing for low speed on a wide range of speeds, in terms of drag reduction. The penalties/benefits depend strongly on the mission profile, but if the aircraft is intended to have a wide variety of mission profiles capability, namely if speed variations are expected, we expect the morphing wing to achieve overall benefits.

In this case, the morphing wing outperforms the original wing at all speeds if airfoil shape change is possible. If not, a morphing wing with the NACA0012 airfoil would be outperformed at low speeds by the original wing, and the stall speed would increase from 15 to 17 m/s. On the other hand, a morphing wing with the Eppler434 airfoil would reduce the stall speed to 14 m/s but would be outperformed by a morphing wing with the NACA0012 at high speeds in terms of drag reduction.

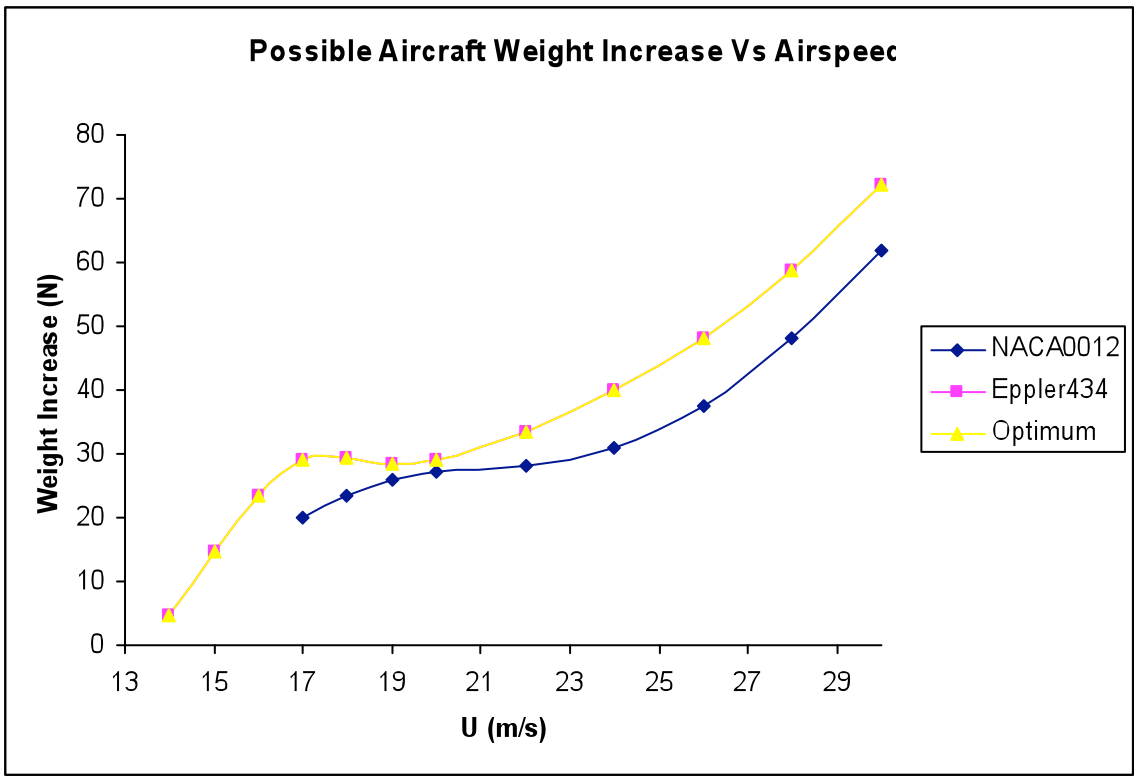

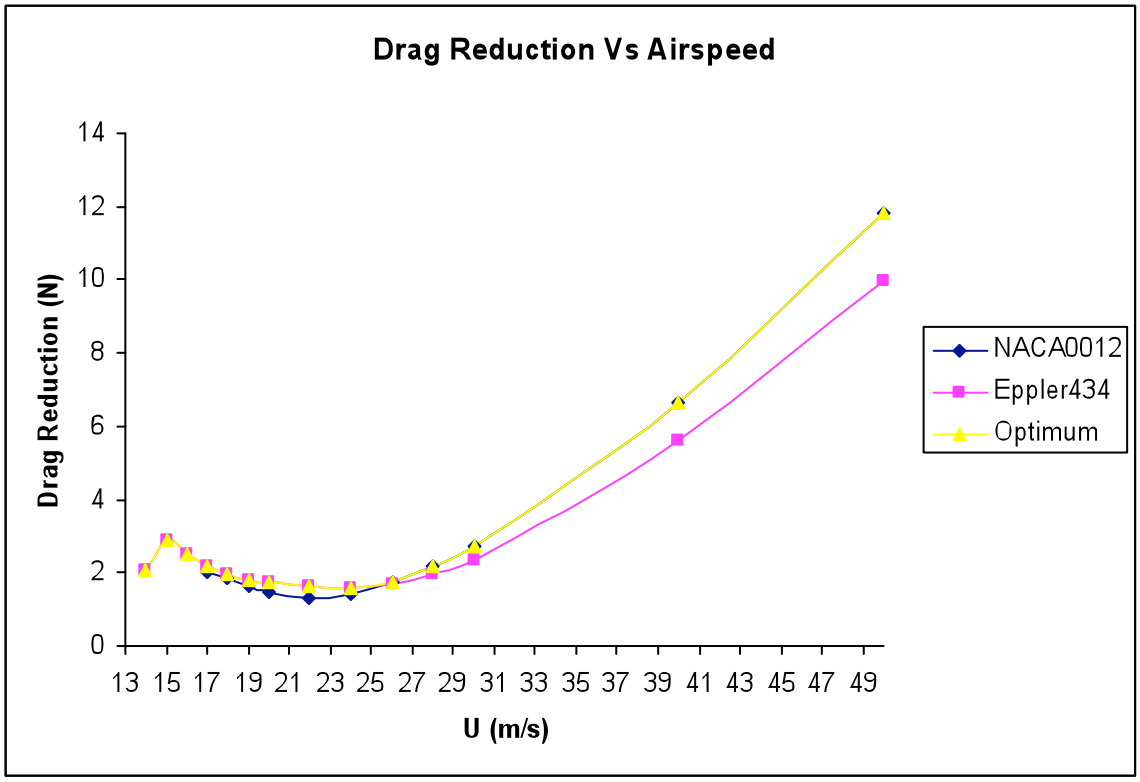

Figure 13: Possible weight increase as a function of take off speed (up) and possible drag

reduction as a function of speed (down) by comparison with the original wing

The graphics show that for the stall speed of 15 m/s of the original RPV wing, the possible weight increase is up to 15 N and the drag reduction of about 3 N, 34% of the original wing drag. For a maximum speed of 50 m/s the drag reduction is 11.8 N. This is a drag reduction of 48.2%

Since the original wing weight is of 14.7 N and the model weight estimate is of 17.0 N, we still have 12.3 N to spare for actuation before the morphing wing weight penalizes the payload at take off.

Experimental Results

The experimental results are based on ground tests and concern mainly actuation speed and energy under loading.

Loading tests intend to simulate conservatively the bending moment on the wing for a 1g loading corresponding to 100 N (50 N for half span). The load is considered distributed on the outer and inner wing based on area proportionality and is considered uniformly distributed on each wing. Loading tests were performed using weights in the wings tips in order to cause equivalent bending moments on the wing's roots.

Final wing weight including actuation mechanisms for span variation and control surfaces was 39 N.

Table 6 shows the measured results.

Table 6. Measured morphing time and energy requirements for different experimental morphing wing loading conditions.

Loading	Outer wing tip load (N)	Inner wing tip load (N)	Total deployment time (s)	Total retraction time (s)	Total deployment energy (J)	Total retraction energy (J)	Max current intensity (A)
0g	0.0	0.0	17.0	17.5	58.14	59.85	0.57
1g	16.0	9.0	18.0	18.5	71.28	73.26	0.66
1.5g	24.0	13.5	19.5	20.0	84.83	87.00	0.88
2g	32.0	18.0	21.5	22.5	110.30	115.43	1.14

Although these measurements were not taken with much precision, they offer a good insight on the order of magnitude of the actuation energy and the actuation time. The type of actuation used doesn't allow fast morphing, the usage of the telescopic capability for roll control is not suitable.

A 2g loading of the structure is possible but close to structural and actuation limit. This means that the stiffness of the composites manufactured is less than the assume stiffness on the computational analysis.

CONCLUSIONS

A morphing telescopic wing concept with airfoil shape change capability was designed and studied computationally through coupled fluid-structure analysis. Strategies for drag reduction morphing with this

concept were obtained and morphing benefits were quantified in terms of possible extra loading and drag reduction. Extra loading at take off speed of 15 m/s was estimated to be 15 N in a 100 N weight aircraft and drag reductions from 1.7 to 12 N, depending on aircraft speed.

An experimental morphing telescopic wing based on the described concept was built and tested on ground to assess construction feasibility and pitfalls, possible improvements in actuation mechanisms and actuation energy.

The experimental morphing wing weight exceeded the extra loading at take off speed in 9 N. It is expected that different construction techniques can reduce wing weight below the threshold of 30 N, therefore obtaining benefits from morphing at low speed flight.

Actuation speed and energy consumption are suitable for quasi static morphing in level flight. Energy consumption indicates that a battery with a 2200 mAh capacity could maintain continuous actuation for at least 1.7 hours when the wing is under 2g loading.

Wing deformation under 2g loading does not compromise structural integrity but may affect aerodynamics due to the hollow outer wing sections deformation.

The leading edge opening of the inner wing is still a functional problem to be solved before flight tests.

Future versions of this morphing wing will reduce wing weight and include airfoil morphing capability.

ACKNOWLEDGEMENTS

This work was possible due to the funding provided to the project SMORPH by the Portuguese FCT (Fundação para a Ciência e Tecnologia) and the funded project POCTI-EME-61587-2004. The author José Vale would like to also thank the Portuguese FCT for the Graduate Fellowship. Additional funding was provided by RTO-NATO Support Program under the framework of the collaborative project PRT-002 between Instituto Superior Técnico, Portuguese Air Force Academy in Portugal and the University of Victoria, in Canada.

REFERENCES

[1] Justin Edward Manzo, “Analysis and design of a hyper elliptical cambered span morphing aircraft wing”, Cornell University, 2006.

[2] P.Bourdin, A.Gatto and M.I. Friswell, “Aircraft Control Via Variable Cant Angle Winglets”, *Journal of Aircraft*, 45 (2):414-423,2008.

[3] Bae J.-S., Seigler T., Inman D. J. and Lee I, “Aerodynamic and Aeroelastic Considerations of a Variable-Span Morphing Wing,” *45th AIAA/ASME/ASCE/AHS/ASC Structures, Structural Dynamics and Materials Conference*, Palm Springs, California, 19-22 April 2004.

[4] Secanell, M., Suleman, A., and Gamboa, P., “Design of a Morphing Airfoil Using Aerodynamic Shape Optimization”, AIAA *Journal*, Vol. 44, No. 7, July 2006, pp. 1550-1562.

[5] J. Hall, K.Mohseni, D. Lawrence and P.Geuzaine. Investigation of variable wing-sweep for applications in micro air vehicles. 2005. AIAA Paper 2005-7171.

[6] J. Vale, P. Gamboa, F. Lau and A. Suleman. Optimization of a morphing wing based on coupled

aerodynamic and structural constraints. 3rd AIAA Multidisciplinary Design Optimization Specialist Conference, 2007.

[7] P. Gamboa, J. Vale, F. Lau and A. Suleman. Multidisciplinary design optimization of a morphing wing for an experimental UAV. 11th AIAA/ISSMO Multidisciplinary Analysis and Optimization Conference, 2006.

[8] P. Aleixo, J. Vale, P. Gamboa, F. Lau and A. Suleman. Design and testing of a morphing wing for an experimental UAV. The Applied Vehicle Technology Panel Symposium (AVT-146), 2007.

[9] J. E. Blondeau and D. J. Pines. Design and testing of a pneumatic telescopic wing for unmanned aerial vehicles. Journal of Aircraft, 44(4):1088-1099, 2007.

[10] Michael Kerho. Adaptative airfoil for dynamic stall control. Journal of Aircraft, 44(4):1350{1360, July-August 2007.

[11] J. S. Flanaganl R. C. Strutzenberg R. B. Myers and E. Rodrian. Development and fight testing of a morphing aircraft the nextgen mfx-1. 48th AIAA/ASME/ASCE/AHS/ASC Structures, Structural Dynamics & Materials Conference, April 2007.

[12] M. H. Love P. S. Zink R.L. Stroud D. R. Bye S. Rizk and D. White. Demonstration of morphing technology through ground and wind tunnel tests. 48th AIAA/ASME/ASCE/AHS/ASC Structures, Structural Dynamics & Materials Conference, April 2007.

[13] José Vale. Designing, building and wind tunnel testing of a morphing wing for drag reduction. Thesis, September 2007.

[14] André Leite. Design of a morphing wing based on Fluid-Structure Interaction analysis. Thesis, September 2008.

[15] J. Bowman B. Sanders B. Cannon J. Kudva S. Joshi and T. Weisshaar. Development of next generation morphing aircraft structures. 48th AIAA/ASME/ASCE/AHS/ASC Structures, Structural Dynamics & Materials Conference, April 2007.

[16] Ivanco G. T. Scott C. R. Love H. M. Scott Z. & Weisshaar T. A. Validation of the Lockheed Martin morphing concept with wind tunnel testing. 48th AIAA/ASME/ASCE/AHS/ASC Structures, Structural Dynamics, and Materials Conference, April 2007.